ELSEVIER

ARTICLE INFO

Article history:
Received 3 October 2011
Received in revised form 27 November 2012
Accepted 1 December 2012
Available online 8 December 2012

ABSTRACT

© 2012 Elsevier B.V. All rights reserved.

1. Introduction

The availability of landslide hazard and risk maps is essential to identify the potential areas of landslide losses and to minimise their societal impact. One of the first steps in this direction is the preparation of a landslide susceptibility map, indicating the relative susceptibility of the terrain for the occurrence of landslides. When combined with temporal information, this can be converted into a landslide hazard map, which can be used in combination with elements at risk information for estimating potential losses due to landslides, and aid long-term landslide risk management in mountainous areas.

A landslide inventory is the basis for any landslide hazard and risk assessment (Carrara and Merenda, 1976; Guzzetti et al., 2000; Brardinoni et al., 2003). A typical landslide inventory map gives information about the type, volume, magnitude, date and place of occurrence. Landslide inventories can be used for the calculation of weights of the pre-disposing factor maps during landslide susceptibility mapping as well as for performance and reliability analysis in prediction modelling (Carrara and Merenda, 1976; Guzzetti et al., 2000; Brardinoni et al., 2003) and in magnitude and frequency analysis for the hazard mapping. However, preparation of landslide inventories by manual methods is a substantial challenge, as it requires time and a team of experienced people. According to an estimate by Galli et al. (2008), preparation of a landslide inventory required is on average one month per interpreter to cover a 100 km^2 area in the Umbria region of Italy. Alternatively, landslide inventories can be prepared through automatic methods by incorporating expert knowledge in image analysis (Barlow et al., 2006; Moine et al., 2009; Martha et al., 2010).

Preparation of semi-automatic landslide inventories can be fast, unbiased and data driven in comparison to manual methods. Particularly with object-oriented analysis (OOA), the outputs are also visually consistent. Recently, Martha et al. (2010) updated landslide diagnostic features using high resolution satellite data and a digital elevation model (DEM), and synthesised them using OOA for landslide detection. They

not only detected landslides accurately but also classified them into translational rock slide, rotational rock slide, shallow translational rock slide, debris flow and debris slide using a semi-automatic method (Martha et al., 2010, 2011). Recent literatures show that many attempts have been made around the globe to prepare landslide hazard maps using manually identified landslides (van Westen et al., 2003; Guzzetti et al., 2005; Pradhan, 2010). Several attempts were made for automatic detection of landslides (Nichol and Wong, 2005; Rosin and Hervas, 2005; Barlow et al., 2006; Borghuis et al., 2007; Martha et al., 2010; Lu et al., 2011). Although it is implicit that the semi-automatic detection of landslides has great potential for short-term goals such as damage assessment after a disaster, evaluation of the applicability of using semi-automatic detection to achieve long-term goals, such as hazard and risk assessment, is worth doing. This research aims to investigate the potential of semi-automatically detected landslides for the preparation of landslide susceptibility and hazard map using statistical methods, which could not be achieved so far in many developing countries due to lack of systematic landslide inventories.

The objective of this paper is to use the multi-temporal landslide inventories, created using OOA, in assessing landslide susceptibility, hazard and risk. In our previous studies (Martha et al., 2010, 2011), we have used time-series images from high-resolution Cartosat-1 (2.5 m), Resourcesat-1 LISS IV Mx (5.8 m) and IRS-1D panchromatic (5.8 m) sensors and prepared landslide inventories for a 13 year period (1997–2009). These multi-temporal inventories in combination with historical daily rainfall data for the same period were used to estimate the spatial and temporal probabilities for hazard assessment. The hazard map was then integrated with data for elements at risk prepared from a high resolution Cartosat-1 image to assess the landslide risk.

2. Materials and methods

2.1. Study area

Countries in the Himalayan region, which is a global hotspot for landslide hazards, frequently face the dangerous outfall of landslides (Nadim et al., 2006). About half a million km^2, i.e. 15% of India's land area is susceptible to landslide hazard. Out of this, 0.098 million km^2 is located in the northeastern region, while the remaining 80% is spread over the Himalayas, Nilgiris, Ranchi Plateau, and Eastern and Western Ghats (GSI, 2006). An area covering 81 km^2 around Okhimath in the Rudraprayag district of Uttarakhand State, including the Garhwal Himalayas along the Rishikesh–Kedarnath tourist and pilgrimage route, was selected for hazard and risk mapping (Fig. 1).

The presence of landslides of different sizes and different types, such as rock slides (rotational and translational), debris slides and debris flows offers a good opportunity to test automatic landslide detection techniques for landslide inventory preparation, and the effect of these inventories on subsequent landslide susceptibility and hazard mapping. Okhimath is situated at an average elevation of 1300 m on the confluence of the Mandakini (originating from Kedarnath) and Madhyamaheshwar rivers. Two major rainfall events, the downpours on 9, 12, 17 and 19 August 1998, and the cloud burst on 16 July 2001 in this area, triggered 466 and 200 landslides, and claimed 103 and 27 lives, respectively (Naithani, 2001; Naithani et al., 2002). Unfortunately, no maps are available showing the spatial distribution of these landslides, and of the damage caused.

2.2. Data

Both multispectral and panchromatic data (Table 1) were used to prepare annual landslide inventories from 1997 to 2009 by OOA. The data sources used for the preparation of evidence layers, which were considered as the most important contributing factors for the occurrence of landslides in the Himalayas, are provided in Table 2. The available geological map prepared by the Geological Survey of India on 1:250,000 scale (Rawat and Rawat, 1998) was used to refine the boundary between different rock types using a break-in-slope criteria (Fig. 2a). This area is traversed by two major thrusts, namely the Main Central Thrust (MCT-II) that passes just south of Okhimath, and the Vaikrita Thrust (also known as MCT-I) that passes north of Okhimath (Fig. 2a). The MCT is a nearly 10 km wide shear zone, inclined at 20° to 45° northward. Foliations dip at moderate angles in NE to NNW directions (Naithani, 2001; Naithani et al., 2002). While thrusts and faults were derived from the available geological map, lineaments were interpreted from LISS-IV Mx and hillshade images (Fig. 2a). Finally, linear geological structures (lineaments, faults and thrusts) were converted to a polygon layer using a variable buffer criterion, since a lineament has a very narrow zone of influence on the strength of the rock in comparison to a thrust, which has larger zone of influence.

The slope angle derived from a 10 m DEM extracted from the stereoscopic Cartosat-1 data, was classified into 10 classes using a quantile classification system. Slope aspects have a significant role for the occurrence of landslides in the Himalayas. South facing slopes support more anthropogenic activities in comparison to other slope directions due to maximum availability of sunlight in a day, leading to the destabilisation of slopes. Therefore, slope aspects derived from the DEM were used for the creation of susceptibility map. Relative relief is another important parameter for the initiation of landslides. It was derived from the DEM using the zonal statistics tool of ArcGIS, wherein slope facets were used as zones (Fig. 2b). Slope facets or terrain units, which have more or less similar characters of slope showing consistent slope direction and inclination, and are generally delimited by ridges, spurs and gullies (Anbalagan, 1992), were prepared manually with the help of the hillshade, slope angle and aspect maps.

The landslides in this area are mainly due to excessive rainfall and less related to the change in land use/cover (Naithani, 2001). As land use has not changed a lot over the period of study, we selected the first available multispectral image in the observation period, i.e. a LISS-IV Mx image of 2004, to prepare the land use/cover map of this area (Fig. 2c). The soil in this area is mostly transported and composed of sub-angular rock fragments with a high proportion of sandy to sandy–silty matrix (Naithani, 2001; Naithani et al., 2002). Soil depth, which is an important parameter for the creation of landslide susceptibility map, was prepared using an available soil map (Fig. 2d) (Atlas, 2001).

2.3. Methodology

The methodology adopted in this chapter for landslide susceptibility, hazard and risk assessment is briefly explained in Fig. 3. The details of the methodology are explained in the following sub-sections.

2.3.1. Preparation of multi-temporal landslide inventories by a semi-automatic method

The knowledge-based semi-automatic method used to create landslide inventories is explained in detail by Martha et al. (2010, 2011). However, for clarity and completeness, the methodology is explained in brief here. All 13 images (Table 1), one corresponding to each year, were processed separately. Multiresolution segmentation of the satellite images was carried out to generate objects, which were used subsequently as image primitives for classification by OOA. A typical effect mostly observed after the occurrence of landslides is loss of vegetation and exposure of bare rock and soil. Therefore, landslide candidates were identified using an NDVI threshold for multispectral images and brightness threshold for panchromatic images. Subsequently, false positives (roads, barren rocky and non-rocky lands, built-up areas, shadows and river sands) were detected. The DEM and its derivatives

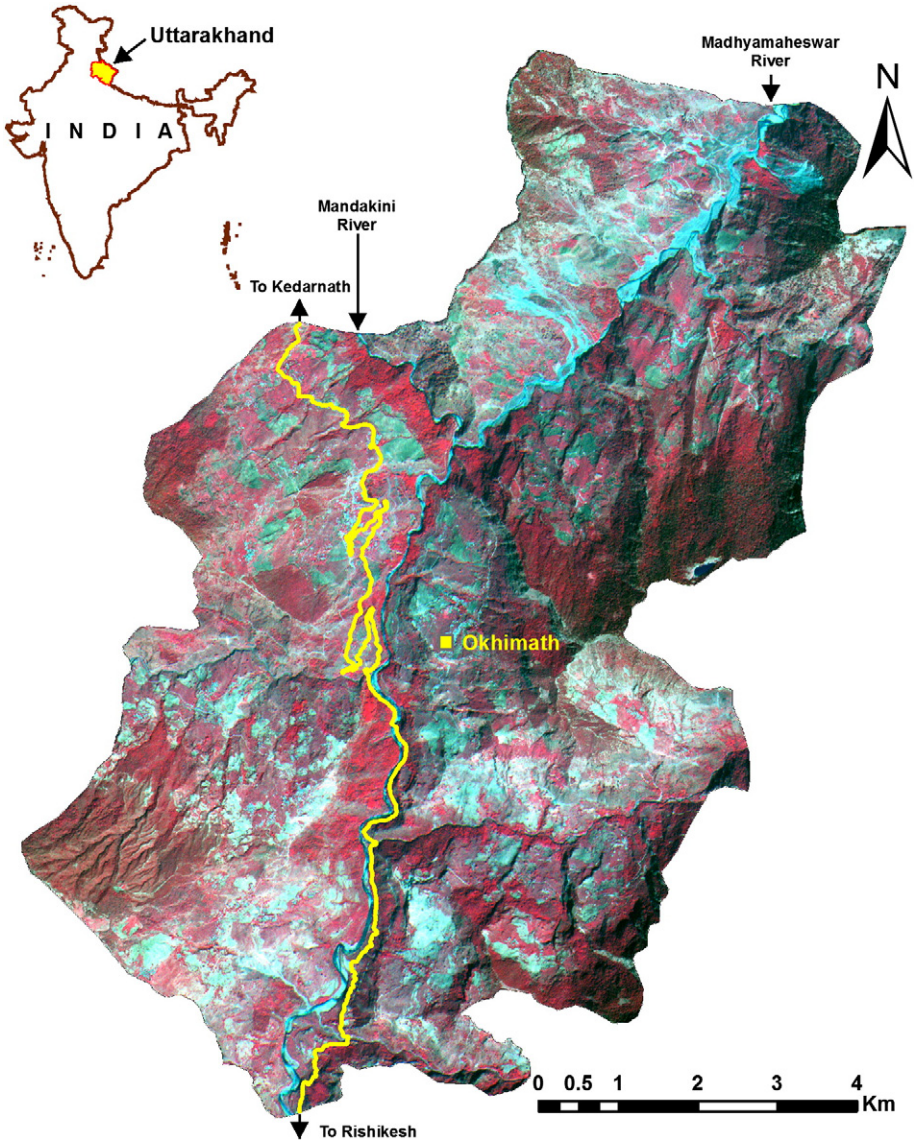

Fig. 1. Location map of the study area shown with Resourcesat-1 LISS-IV Mx image (01 April 2007). The yellow line indicates the main road (NH-109) in the valley.

(slope, hill shade and flow direction), critical to the successful detection of landslides, were used in the analysis. Landslides were classified based on the type of material and movement mechanism by using terrain curvature and adjacency conditions.

We used two images corresponding to the year 1998 (Table 1). The results obtained from the image dated 14 April 1998 can be assumed as the inventory corresponding to the landslides triggered during the monsoon of 1997, since July and August are the wettest months in this area, where rainfall is the major triggering event

Table 1
Details of the high resolution satellite data used for the preparation of historical landslide inventories.

Satellite data	Resolution (m)	Date of acquisition
IRS-1D PAN	5.8	14 April 1998
		02 November 1998
		21 September 1999
		28 May 2000
		24 March 2001
		14 November 2002
		13 April 2003
		13 Mar 2005
Cartosat-1 PAN	2.5	06 April 2006
Resourcesat-1 LISS-IV Mx	5.8	16 April 2004
		01 April 2007
		15 December 2008
		28 October 2009

Table 2
List of evidence layers and their sources used to derive landslide susceptibility.

Evidence layers	Number of classes	Data sources
Lithology	4	Geological map on 1:250,000 scale, updated using Resourcesat-1 LISS-IV Mx and DEM
Geological structure	2	Geological map on 1:250,000 scale, Resourcesat-1 LISS-IV Mx and Hillshade
Soil depth	4	Soil map on 1:50,000 scale
Land use/Land cover	8	Resourcesat-1 LISS-IV Mx
Slope angle	10	10 m DEM
Slope aspect	9	10 m DEM
Relative relief	5	10 m DEM and slope facet

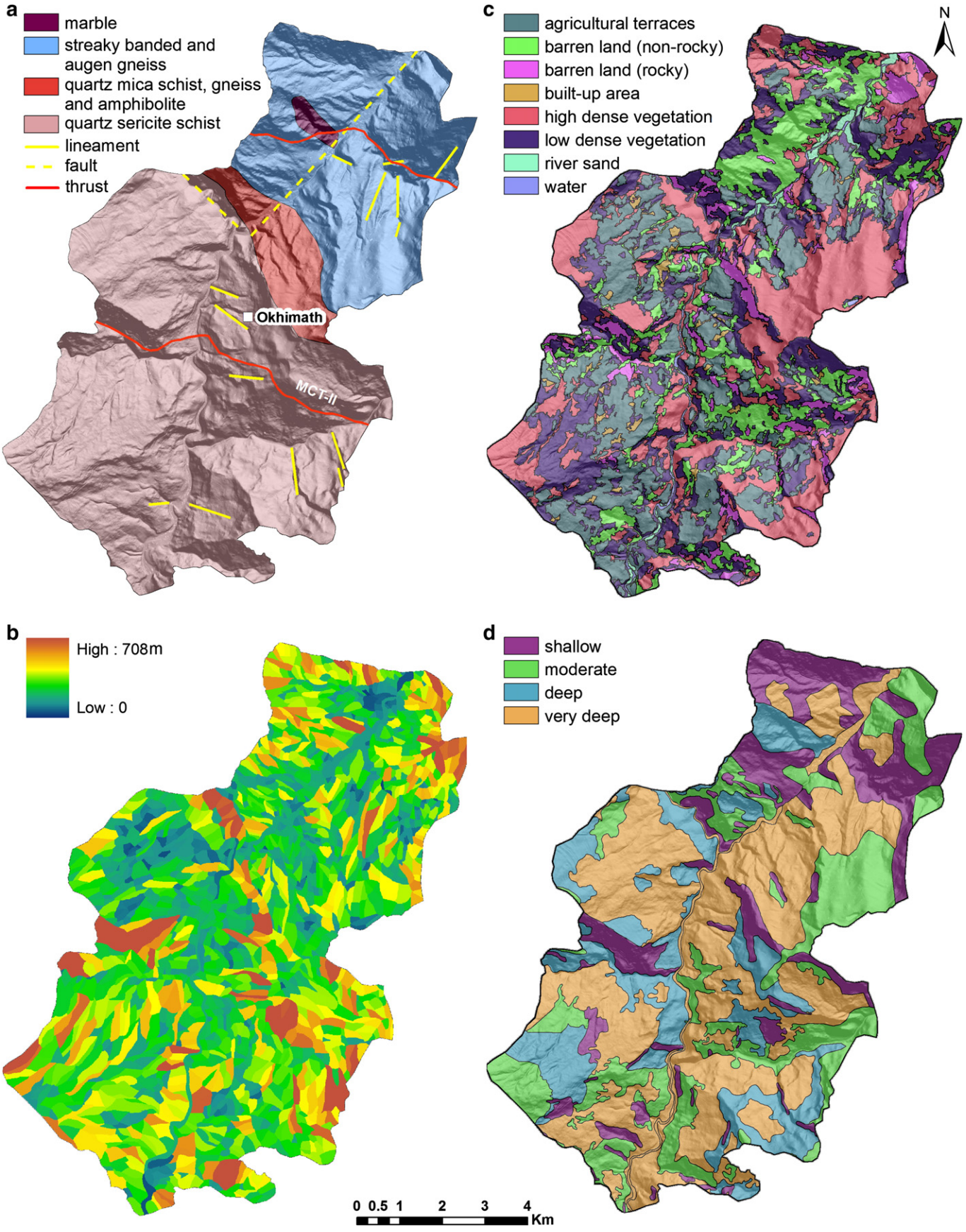

Fig. 2. Some of the important evidence layers used for preparation of landslide susceptibility map. (a) Lithology and structure (updated using a quadrangle geological map published by GSI). (b) Relative relief. (c) Land use/cover. (d) Soil depth.

(Fig. 4). Thus we have a continuous landslide inventory with annual landslide inventories for 13 years (1997–2009). The maximum and minimum detection percentage of all landslides, which was calculated by comparing the semi-automatically detected landslides with manually identified landslides for the total period, were 96.7% and 71.5%, respectively (Martha et al., 2012). Corresponding quality percentages, which indicate how likely the landslides detected by the semi-automatic method is true, are 88.1% and 55.3%, respectively (Martha et al., 2012). However, the landslide inventories prepared by semi-automatic methods, particularly those prepared from panchromatic images, sometimes have a high error of commission, i.e. non-landslide areas were falsely identified as landslides. The majority of the false positives were masked out, after visual inspection, by applying specific rules based on landslide patterns from the previous year, land use, slope and lithology.

2.3.2. Generation of the landslide susceptibility map

One of the first and most important steps involved in landslide hazard mapping is the assessment of landslide susceptibility, which indicates the spatial distribution of localities that are favourable for future occurrence of landslides. The susceptibility map shows the proneness of an area to landslides. The susceptibility map can be prepared in a GIS using statistical, heuristic or physically-based methods (Guzzetti et al., 2005). With heuristic methods, weights are assigned to the predisposing factors also known as causative factors or evidence layers, based on the experience of the experts, whereas in data driven statistical techniques, weights are obtained by correlating landslide occurrences and evidence layers, using both univariate and multivariate methods. Commonly used bivariate methods are information-value and weights-of-evidence modelling in which weights for each parameter are derived from the landslide inventory (Mathew et al., 2007). Since the objective of this paper is to verify the effectiveness of semi-automatically prepared landslide inventories in susceptibility, hazard and risk mapping, we decided to use a relatively simple method (weights-of-evidence) in order to analyse the relation of each annual inventory map with the causative factors.

The method 'weights-of-evidence' or *wofe* was initially developed for the identification and exploration of mineral deposits using borehole or geochemical data (Bonham-Carter et al., 1989; Carranza and Hale, 2003). Many researchers, such as Mathew et al. (2007), Neuhäuser and Terhorst (2007), Poli and Sterlacchini (2007), Thiery et al. (2007) and Ghosh et al. (2009) have used it also for landslide susceptibility assessment. In this method, historical landslides are used to calculate weights of evidence layers to demarcate future areas of landslides under the assumption that similar factors will prevail in future also (Neuhäuser and Terhorst, 2007). The main assumption of *wofe* is that the evidence layers are independent of each other. The method nevertheless provides relatively easy and understandable results, and has proven to be a useful exploratory tool in susceptibility assessment, for subdividing the terrain into classes with similar susceptibility, rather than for using the actual posterior probability values which are often too high, due to the conditional dependence of the factors. By overlaying landslide locations with each evidence layer, a pair of weights, i.e. W^+ and W^-, are calculated for each class in each layer, which are indicative of the spatial relationship between the landslides and evidences. This calculation is done by applying likelihood ratios, which describe the probability of occurrence of landslides in the presence and absence of evidences. The end product of this analysis is a map showing the relative proneness of the terrain to produce landslides i.e. landslide susceptibility.

In this study, we used ArcSDM software, a geoprocessing tool of ArcGIS 9.3.1 for the *wofe* analysis (Sawatzky et al., 2009). This software automatically calculates positive and negative weights (W^+ and W^-) depending on the association between the response variable (landslides) and each class of predictor variables (evidence layers). The contrast (C) and studentised contrast (sC) calculated by the software are useful to understand the spatial association of each class of predictor variables and response variable (Poli and Sterlacchini, 2007). Since the software accepts response variables as points, landslide inventories created as polygons were converted to grids (50×50 m), using the method applied by Poli and Sterlacchini (2007). Subsequently, the inventory grids were converted to points, resulting in representation of one landslide by a number of points depending on its size. One common and frequently used practice in landslide modelling is to develop a model using one time period inventory and validate it with the inventory of the next time period. Therefore, a temporal sub-setting of the landslide inventory database was made to create the training and testing data for the *wofe* analysis. Landslide inventories up to the year 2004 were treated as training data, whereas those from 2005 until 2009 were treated as testing data. While the training points were used to calculate the weights of the evidence layers, testing points were used to validate the usefulness of *wofe* model in predicting future landslides. The landslide susceptibility map was classified into high, moderate and low susceptibility categories using the success rate curve of the *wofe* model.

2.3.3. Landslide hazard estimation

After the susceptibility map was prepared, the next step was to assess the landslide hazard. This was done by calculating the temporal probability of landslide occurrence within the landslide susceptible areas. To estimate the spatial and temporal probabilities, annual landslide inventories prepared by the semi-automatic method and historical daily rainfall data were used.

The spatial probability corresponding to each inventory year and for all the three susceptibility classes was calculated separately by ratioing the areas using the following equation:

$$\text{spatial probabilty} = \frac{\text{area of landslides}}{\text{area of susceptibility class}}. \quad (1)$$

We used the annual maximum daily rainfall amount over 13 years for the frequency analysis of extreme events using the method described by Gumbel (1958), which is used frequently in hydrological applications (Jaiswal et al., 2011). The Gumbel extreme model can be applied to model the probability of occurrence of the rainfall event (N_R) equal to or less than some value n. The model can be expressed as:

$$P(N_R \leq n) = e^{-e^{-(\alpha+n)/c}} \quad (2)$$

where α and c are two parameters of the Gumbel distribution. By the method of moments, the parameters are evaluated as (Chow et al., 1988):

$$\alpha = \gamma c - c \quad (3)$$

$$c = \frac{\sqrt{6}}{\pi}\sigma \quad (4)$$

where $\gamma = 0.57721$ is a Euler's constant and σ is the standard deviation. For a specified time interval in a year, Eq. (2) can be rewritten for the value (N_R) equal to or greater than some value n as:

$$P(N_R \geq n) = \frac{1}{T} = 1 - e^{-e^{-(\alpha+n)/c}} \quad (5)$$

where T is the return period of the rainfall event. Two methods are commonly used for fitting distributions to the Gumbel model for frequency analysis; i) the plotting position method, and ii) the frequency factor method. The former is a simple method to obtain the distribution function by the use of certain "plotting position" formula (Chow et al., 1988). The technique is used to arrange the data in an increasing or decreasing order of magnitude and to assign the order number R to the ranked values. The Weibull formula is commonly used to obtain the plotting position, and that for $P(N_R \geq n)$ can be expressed as:

$$P = \frac{R}{m+1} \quad (6)$$

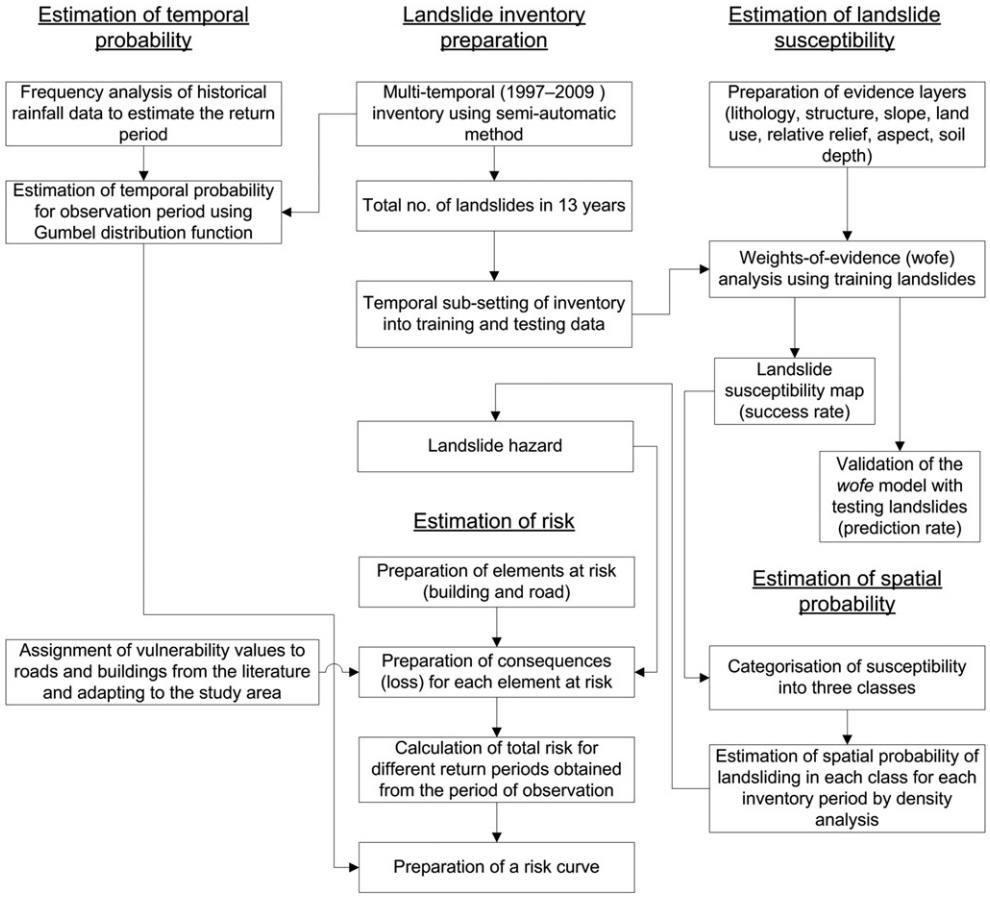

Fig. 3. Procedure for landslide hazard and risk assessment using semi-automatically prepared landslide inventory maps.

where R is the rank and m is the total number of observations. When R is ranked from the lowest to highest, P is an estimate of $P(N_R \leq n)$; when the rank is from the highest to lowest, P is $P(N_R \geq n)$. Eq. (6) can be plotted on a probability chart to represent the cumulative probability distribution. The graph is designed in such a way that it gives the return period for a magnitude of event. In this study, $m = 13$. The rainfall values were ranked from low to high, with the lowest rank (1) assigned to the lowest rainfall value and the highest rank (13) assigned to the highest rainfall value. Using the plotting position method, the data were plotted on a probability chart and a curve was fitted to the plotted points. Then the return period for each of four scenarios (daily rainfall amount of 50, 100, 150 and 200 mm) was measured from the fitted curve. We selected the four scenarios considering the minimum and maximum annual daily rainfalls for the landslide inventory period (1997–2009): 23.4 and 204 mm, respectively.

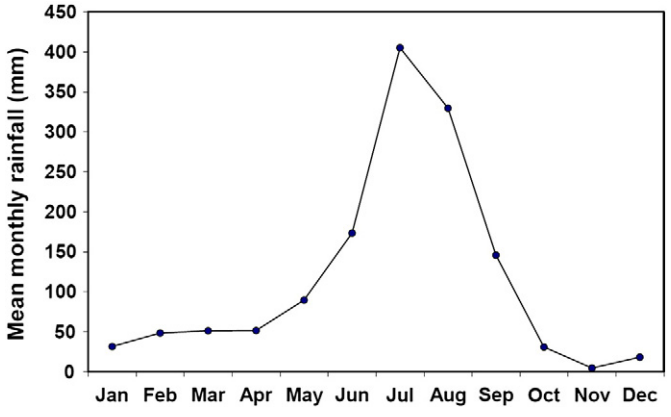

Fig. 4. Mean monthly rainfall pattern in the study area for 34 years (1976–2009). Source: Central Water Commission, Dehradun, India.

2.3.4. Landslide risk estimation

Landslide risk can be defined as the expected number of lives lost, persons injured, damage to properties and disruption of economic activities due to landslides for a given area and a reference period (Varnes, 1984). The concept of risk that has been applied to landslide studies can be expressed by the following generic equation (van Westen et al., 2006; Zêzere et al., 2008):

$$\text{landslide risk} = \text{landslide hazard} \times \text{vulnerability} \times \text{value of exposed elements at risk.} \quad (7)$$

In the previous section, we have explained how the landslide hazard can be estimated quantitatively. In this study we focused on buildings and roads as elements at risk, which were mapped through visual interpretation of Cartosat-1 images. The buildings were categorised into nine occupancy classes based on field verification. Further, each building was classified into good, regular and bad in terms of its structural condition based on building sample surveys.

Most of the houses in the study area are confined to two localities, i.e. Okhimath and Guptakashi. The houses there are reinforced with concrete and well constructed. Other parts of the study area are in a rural environment with small isolated clusters of houses, which are not well constructed. It was not possible to map the daily movement of population or the number of people living in each house for such a large area. Therefore, the risk assessment was carried out for houses and not the population.

Vulnerability is possibly the most difficult term to represent quantitatively within landslide risk analysis (van Westen et al., 2008; Zêzere

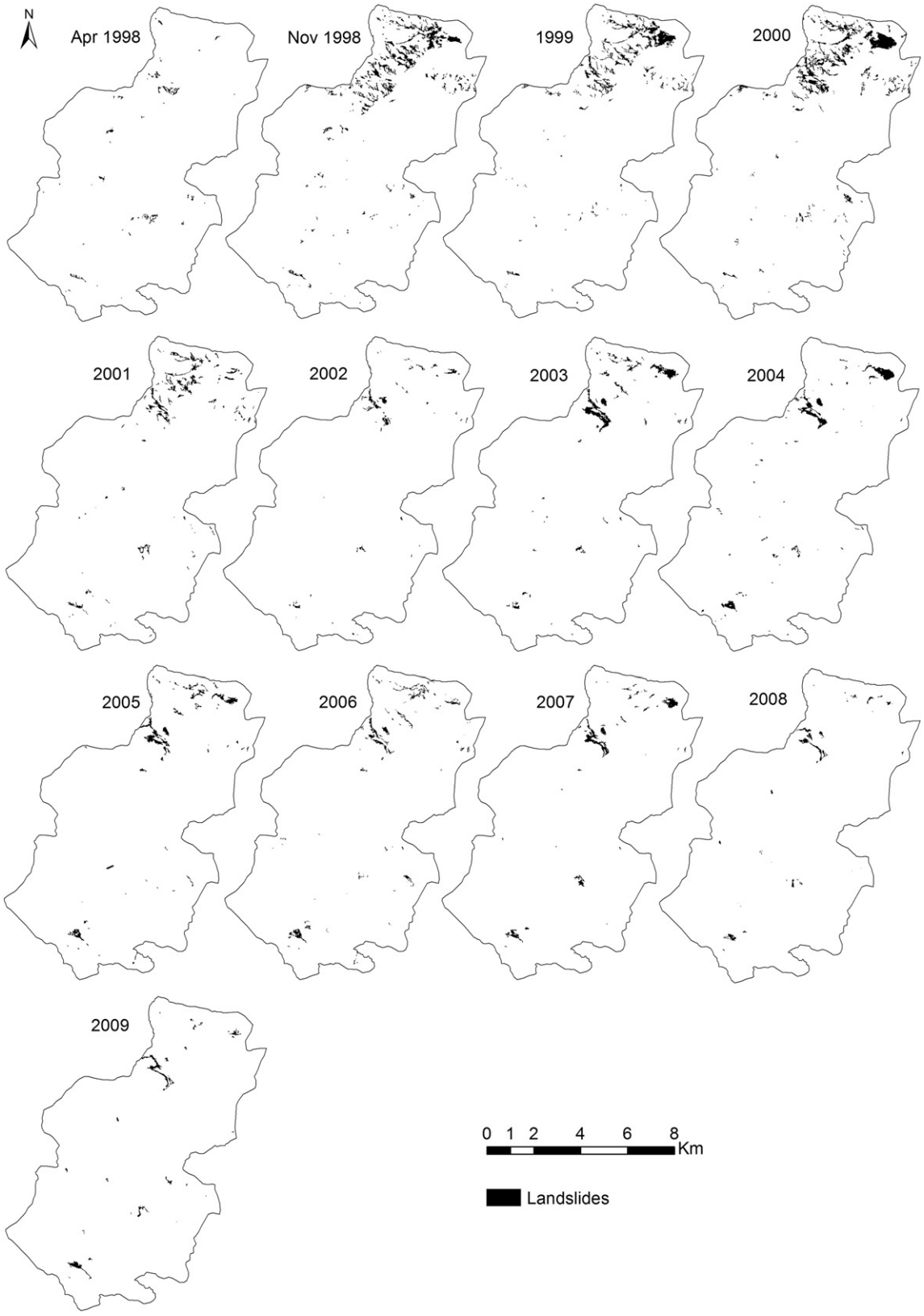

Fig. 5. Semi-automatically prepared annual landslide inventories for 1998–2009 period. While landslide inventories from 1998 to 2004 were used as training dataset for the *wofe* model, inventories from 2005 to 2009 were used as testing dataset.

et al., 2008). Vulnerability depends on landslide type, magnitude and type of risk element exposed, and its estimation requires data of past damage (Fuchs et al., 2007; Papathoma-Kohle et al., 2007). Reliable estimates of vulnerability for a specific element at risk are rare, though in the literature vulnerabilities for particular conditions have been suggested (Glade, 2003; Bell and Glade, 2004). Considering the landslide type in this area and consulting the literature, vulnerability values between 0.3 and 1 were assigned to the different types of building

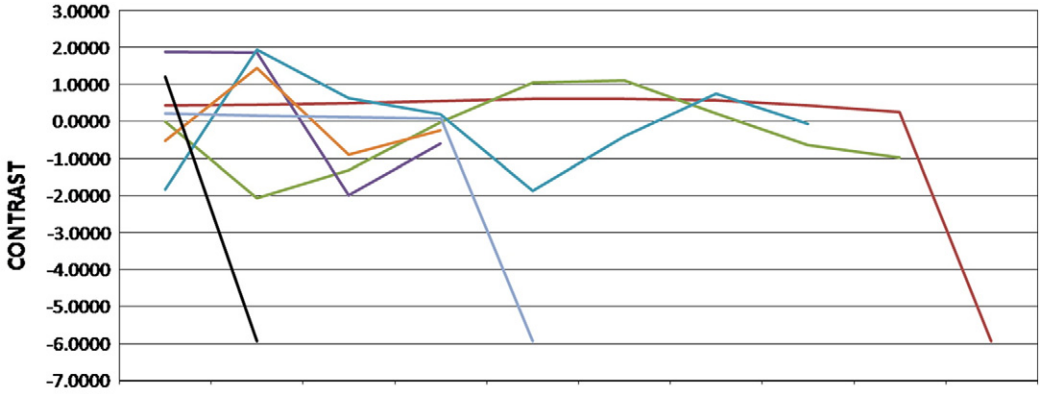

slope	47°-89°	41°-47°	36°-41°	32°-36°	28.5°-32°	25°-28.5°	21.5°-25°	18°-21.5°	13°-18°	0°-13°
aspect	Flat	N	NE	E	SE	S	SW	W	NW	
lithology	Mar	SBAG	QSS	QMSGA						
landuse	AT	BL (NR)	BL (R)	BA	HDV	LDV	RS	W		
soil depth	Moderate	Shallow	Very deep	Deep						
relative relief	0-130	130-202	202-288	288-408	408-709					
structure	Close	Far								

Fig. 6. Contrast values for all classes of the seven evidence layers. Lithology (Mar: marble, SBAG: streaky banded and augen gneiss, QSS: quartz sericite schist, and QMSGA: quartz mica schist, gneiss, amphibolite), land use (AT: agricultural terraces, BL (NR): barren land (non-rocky), BL (R): barren land (rocky), BA: built-up area, HDV: high dense vegetation, LDV: low dense vegetation, RS: river sand and W: water).

(Castellanos Abella, 2008). The cost of the building and the vulnerability were estimated for each building type. The vulnerability map was multiplied on a cell by cell basis with the spatial probability of landslides for the return period of four rainfall scenarios (50, 100, 150 and 200 mm) in order to estimate the building risk.

The study area has a good road network, as the access to the origin of the river Ganges is of national importance. The national highway (NH-109) passing through this area is very busy, particularly during the tourist season. Absolute vulnerability values (representing the expected reconstruction costs per unit length of road) were assigned to the highway and district road, respectively, based on Nayak (2010). The absolute vulnerability was multiplied with the spatial probability on a cell by cell basis, the sum of which for a given return period estimates the risk to the road.

Total risk for a given return period of rainfall intensity was calculated by summing up the risk to the buildings and roads. In this manner landslide risk for four rainfall scenarios was estimated separately.

Table 3
List of evidence classes showing a positive correlation. Studentised contrast (*sC*) is a measure of the correlation significance.

Evidence layer	Class	W^+	W^-	*sC*
Slope	47°–89°	0.3868	−0.0505	6.9791
	41°–47°	0.3641	−0.1099	9.7745
	36°–41°	0.3324	−0.1784	11.5885
	32°–36°	0.3064	−0.2598	13.0476
	28.5°–32°	0.2684	−0.3503	13.7068
	25°–28.5°	0.2068	−0.4170	12.7178
	21.5°–25°	0.1429	−0.4337	10.5914
	18°–21.5°	0.0758	−0.3708	7.1558
	13°–18°	0.0226	−0.2377	3.1994
Structure	Close to fault, thrust and lineament	0.5169	−0.6858	25.2137
Lithology	Marble	1.8394	−0.0405	18.2082
	Streaky banded and augen gneiss	0.9380	−0.9215	38.8269
Land use	Barren land (non-rocky)	1.2728	−0.6658	44.2759
	Barren land (rocky)	0.5721	−0.0525	9.0118
	Built-up area	0.1967	−0.0024	1.0450
	River sand	0.7478	−0.0113	5.0240
Soil depth	Shallow	0.9930	−0.4508	33.2545
Aspect	Southeast	0.8352	−0.2190	22.3148
	South	0.9127	−0.2087	23.1966
	Southwest	0.2123	−0.0188	3.0571
Relative relief	0–130 m	0.1677	−0.0460	4.1723
	130–202 m	0.0890	−0.0624	3.4611
	202–288 m	0.0424	−0.0672	2.4466
	288–408 m	0.0147	−0.0627	1.3851

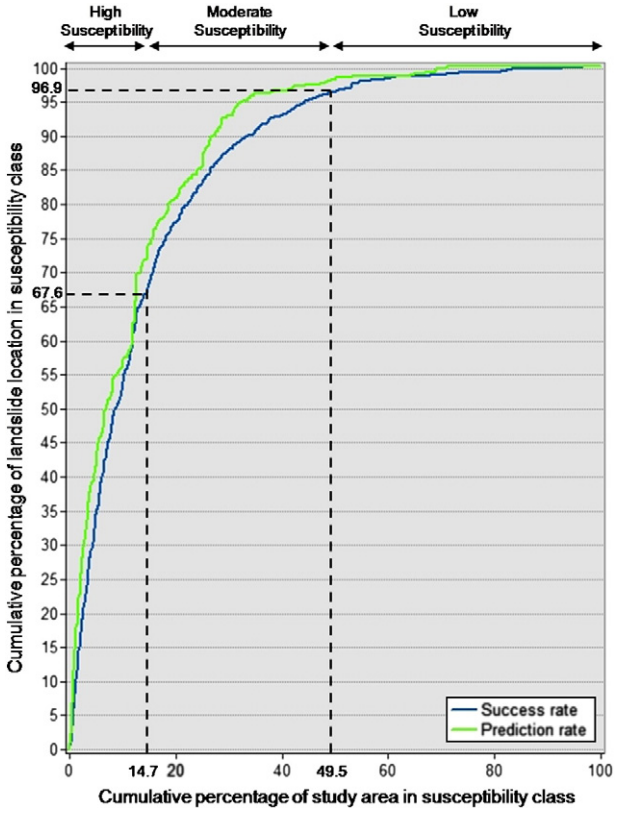

Fig. 7. Performance of the *wofe* model for landslide susceptibility mapping in the Okhimath area. The curves show the success and prediction rates of the model.

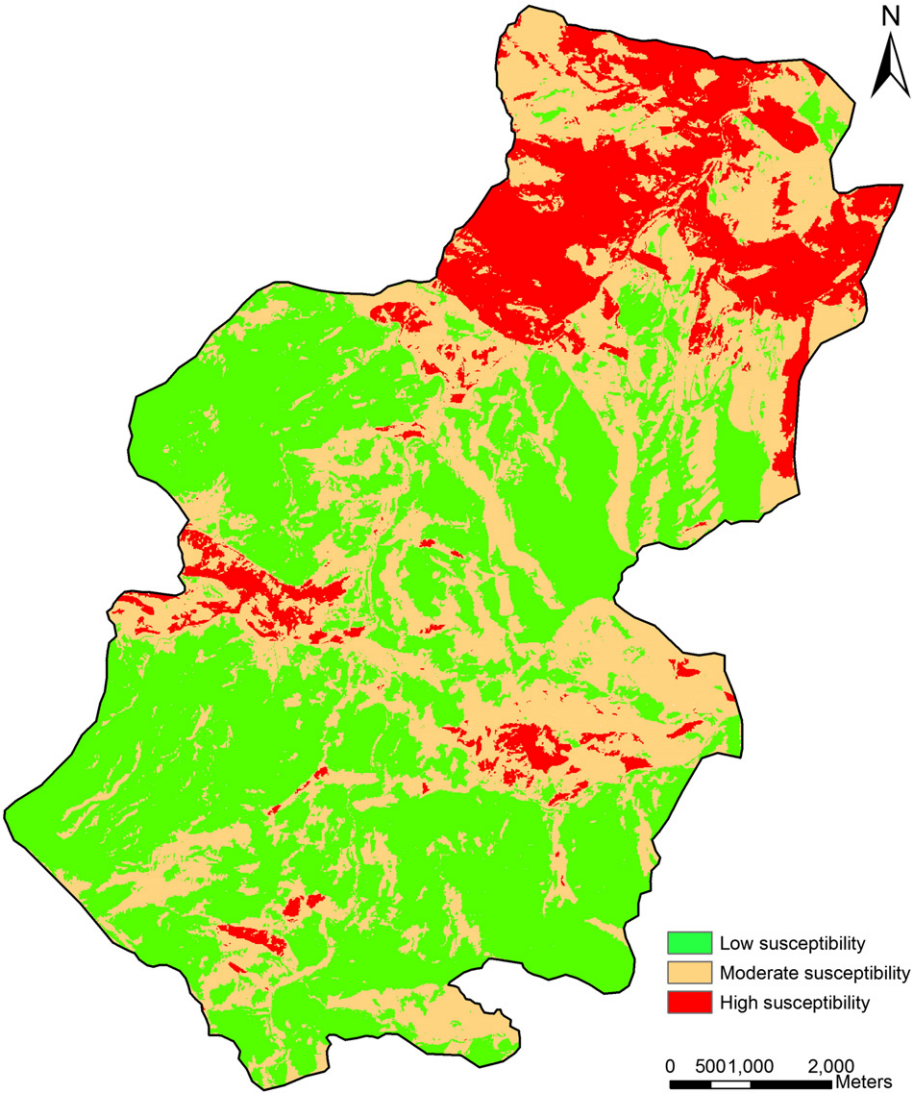

Fig. 8. Landslide susceptibility map of the Okhimath area prepared using the *wofe* model.

Finally, a risk curve was plotted showing the relation between the annual probability and consequences to estimate the annualised loss.

3. Results and discussion

3.1. Landslide susceptibility assessment

Using ArcSDM software, *wofe* analysis was performed. A total of seven evidence layers and 2137 response variables, i.e. landslide points in a 50×50 m grid corresponding to the inventory from 1997 to 2004 (Fig. 5), were used to calculate the weights. The evidence layers were converted to a 10×10 m grid for the *wofe* analysis, since a 10 m DEM was used in this study for derivation of the topographic layers.

Fig. 6 shows a comparison of contrast values ($W^+ - W^-$) of all evidence classes. This is an important measure of correlation between the landslide locations and evidence layers. Table 3 summarises only the evidence classes that were positively correlated. Although the slope classes from 13° to 89° have a consistent contrast, the *sC* values of the five slope classes from 21.5° to 41° were relatively high compared to the other classes, showing that these slopes were significant for the occurrence of landslides. Among the lithological units, streaky banded and augen gneiss has the highest *sC* value. This unit, which is mainly exposed in the Madhyamaheshwar Valley along with the MCT was responsible for high occurrence of landslides. Non-rocky barren land has both the highest contrast (Fig. 6) and *sC* (Table 3), indicating that it was the most critical land use class for the high occurrence of landslides. South-facing slopes are known for their landslide proneness in the Himalayas. This was revealed clearly by the *wofe* model, since it has only shown positive correlation among all other aspect classes. Areas with high relative relief in the Himalayas are mostly exposed as rocky escarpments consisting of hard rock and

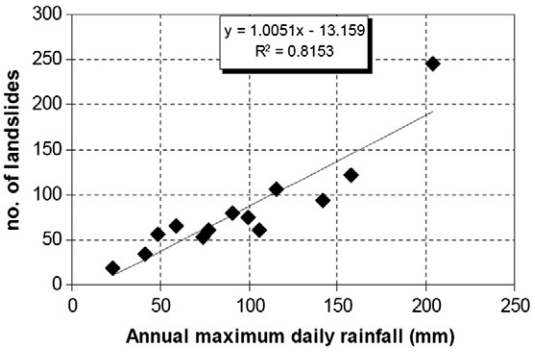

Fig. 9. Relationship between the number of landslides (1997–2009) and daily maximum rainfall.

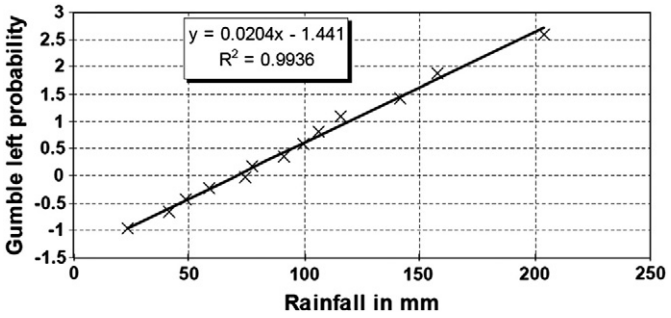

Fig. 10. Gumbel plot for estimating the return period.

are mostly stable. Therefore, only areas with low relative relief had shown positive correlation with landslides.

Finally, overlay of all weighted factors and calculation of the overall susceptibility scores were carried out. The cumulative percentage of landslide location was plotted against the cumulative percentage of the area to create a success rate curve in order to classify the study area for its landslide susceptibility. Fig. 7 shows the success rate curve in which two inflection points were identified for classifying the area into three susceptibility classes. The first inflection point is at 67.6 cumulative percentages of all landslides, corresponding to 14.7 cumulative percentage of the total study area. The second inflection point is at 96.9 cumulative percentages of all landslides, corresponding to 49.5 cumulative percentage of the total study area. It means 67.6% and 29.3% of all landslides, and 14.7% and 34.8% of the total, are in the high and moderate susceptibility classes, respectively. The remaining part of the study area is in the low susceptibility category (Fig. 8).

The prediction rate curve was created using 713 testing landslide points (corresponding to the landslide inventory for the period 2005 to 2009). The prediction rate curve showed a good match with the success rate curve, indicating that the *wofe* model and the seven selected evidence layers were able to predict correctly the spatial occurrence of landslides (Fig. 7).

3.2. Landslide hazard assessment

The spatial probability of landslide occurrence for each observation year was estimated for the three susceptibility classes using Eq. (1). Previous researchers, such as Ghosh et al. (2012a,b) have shown that discriminate analysis (DA) is useful to establish a relationship between landslide events and various rainfall predictors in a data scarce environment, and the frequency of predicted landslides events can be used in a Poisson's distribution model to calculate the temporal probability. We attempted DA to establish the relationship, but the cross validation results were not significant due to a small number of known landslide event days in our study area. Instead, the relationship is shown with a linear regression analysis, between daily maximum rainfall and the landslide event (Fig. 9). Daily maximum rainfall was preferred over other rainfall variables for two reasons; i) daily maximum rainfall data matched with the date of occurrence of some historic landslide events available in the literature (Naithani, 2001), and ii) the landslide inventories used in this study are annual inventories, and not event-based ones. According to Naithani (2001), the August, 1998 rainfall event mainly triggered debris slides and rock slides of translational and rotational types. Therefore, we used daily maximum rainfall to estimate the temporal probability of all types of landslides in this case study.

For estimating temporal probability, daily maximum rainfall for 13 years was analysed using Gumbel analysis. The resultant Gumbel plot is shown in Fig. 10. The trend line in this plot was used to estimate the temporal probability of the landslides for four rainfall scenarios (50, 100, 150 and 200 mm). Table 4 shows the estimated annual probabilities for the four scenarios.

Table 4
Annual probabilities of landsliding for four scenarios derived from Gumbel analysis.

Rainfall scenario	Gumbel y-axis value	Return period (years)	Annual probability
50 mm	−0.42	1.3	0.76
100 mm	0.59	2.3	0.43
150 mm	1.61	5.5	0.18
200 mm	2.63	14	0.17

3.3. Risk assessment

Risk assessment for buildings and roads was carried out separately, before both were added to estimate the total risk due to landsliding in the Okhimath area. Although Naithani (2001) provided some details of the 1998 Okhimath disaster including the reported damage to roads and houses and the number of casualties, they are not available in the form of spatial data. We created 2211 building foot prints through stereoscopic interpretation of the high resolution Cartosat-1 data. We categorised the buildings according to their occupancy class, material types (reinforced masonry and wooden buildings) and state of conservation in order to assign vulnerability values. The buildings in the Okhimath area are mostly of reinforced concrete and either with a single storey or two floors. Therefore, we have classified the buildings as good, regular and bad conditions and applied the vulnerability values as proposed by Castellanos Abella (2008). Table 5 lists the category of buildings and their corresponding vulnerability values. The average cost of the buildings in the hilly terrain according to the Border Road Organisation (BRO) was multiplied with the spatial probability and vulnerability to estimate the total building losses. Using the relationship shown in Fig. 9, the number of landslides was estimated for the four rainfall scenarios. We assume that the landslides for each rainfall scenario will be spatially distributed in the same manner as our inventoried data. For example, for the scenario of 100 mm rainfall return period, we assumed the spatial distribution of landslides will be equivalent to the landslide inventory for the year 1997 with recorded a daily maximum rainfall of 99.7 mm.

For the estimation of risk to the roads, stereoscopic interpretation of satellite data was performed for a total road length of 105 km, consisting of a national highway and district roads, was mapped. The cost of reconstruction of completely damaged roads according to the records of the BRO, is Indian rupees 7 lakhs (15,910 US$) per kilometre (Nayak, 2010). The absolute vulnerability of each road type was multiplied with a landslide probability on a cell by cell basis and summed to estimate the total loss due to landslides for the four scenarios.

Finally, the building and road losses were summed and then plotted against the annual probability of landslide occurrence to obtain a risk curve (Fig. 11). The curve does not follow the ideal concave shape, reflecting uncertainty in vulnerability quantification and non-consideration of some elements at risk.

Table 5
Building categories in the Okhimath area and their vulnerability values based on the literature.

Building category (total number)	Good	Regular	Bad
Educational institution (6)	0.3	–	–
Guest house/hotel (11)	0.4	–	–
Hospital (2)	0.4	–	–
Shop (50)	0.4	0.6	0.8
Petrol filling station (1)	0.3	–	–
Place of worship (3)	0.3	0.6	–
Police station (1)	0.3	–	–
Post office (1)	0.4	–	–
Residential (2135)	0.5	0.8	1
Telephone exchange (1)	0.4	–	–

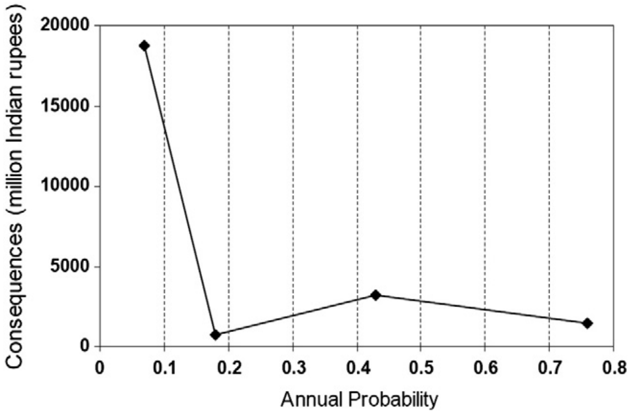

Fig. 11. Total risk (building and road) due to landslide in the Okhimath area.

4. Conclusions

This paper has demonstrated the use of a semi-automatically prepared landslide inventory from high resolution images in landslide hazard and risk assessment. The landslide susceptibility map was prepared using the established *wofe* model. This was possible because the multi-temporal semi-automatic outputs derived by OOA were georeferenced to a common spatial framework and were available in a GIS-ready format. The matching of the prediction rate curve with the success rate curve indicated that semi-automatically prepared landslide inventories were useful in deriving weights of the evidence layers essential for landslide susceptibility mapping. The results were on a par with the susceptibility map from inventories prepared in a different manner (e.g. field based or manually interpreted from images). The seven evidence layers for our landslide susceptibility assessment were selected based on their high contribution to landsliding, which was also highlighted in previous studies. The present study validates the importance of these layers. Although temporal sub-setting of landslide inventories was attempted, susceptibility assessment using the inventory map of a certain year, and calculation of prediction rate using the inventory of the subsequent year would be worth doing in future. For the estimation of temporal probability, daily maximum rainfall data were used. It will be good if other rainfall variables such as several-day antecedent rainfall can also be used. Although only two elements at risk were considered in this study, it allowed us to evaluate landslide risk in general. More realistic assessments of vulnerability based on the details of previous damages will improve the quality of the landslide risk curve.

Acknowledgements

References

Anbalagan, R., 1992. Landslide hazard evaluation and zonation mapping in mountainous terrain. Engineering Geology 32, 269–277.

Atlas, 2001. Landslide Hazard Zonation Mapping in the Himalayas of Uttaranchal and Himachal Pradesh using Remote Sensing and GIS Techniques. National Remote Sensing Agency, Department of Space, Government of India, Hyderabad, India.

Barlow, J., Franklin, S., Martin, Y., 2006. High spatial resolution satellite imagery, DEM derivatives, and image segmentation for the detection of mass wasting processes. Photogrammetric Engineering and Remote Sensing 72, 687–692.

Bell, R., Glade, T., 2004. Quantitative risk analysis for landslides — examples from Bíldudalur, NW-Iceland. Natural Hazards and Earth System Sciences 4, 117–131.

Bonham-Carter, G.F., Agterberg, F.P., Wright, D.F., 1989. Weights of evidence modelling: a new approach to mapping mineral potential. Statistical Application in Earth Sciences 89, 171–183.

Borghuis, A.M., Chang, K., Lee, H.Y., 2007. Comparison between automated and manual mapping of typhoon-triggered landslides from SPOT-5 imagery. International Journal of Remote Sensing 28, 1843–1856.

Brardinoni, F., Slaymaker, O., Hassan, M.A., 2003. Landslide inventory in a rugged forested watershed: a comparison between air-photo and field survey data. Geomorphology 54, 179–196.

Carranza, E.J.M., Hale, M., 2003. Evidential belief functions for data-driven geologically constrained mapping of gold potential, Baguio district, Philippines. Ore Geology Reviews 22, 117–132.

Carrara, A., Merenda, L., 1976. Landslide inventory in northern Calabria, southern Italy. Geological Society of America Bulletin 87, 1153–1162.

Castellanos Abella, E.A., 2008. Multi-scale Landslide Risk Assessment in Cuba. ITC dissertation 154 Thesis, Utrecht University, Utrecht, 273 pp.

Chow, V.T., Maidment, D.R., Mays, L.R., 1988. Applied Hydrology. McGraw-Hill, New York.

Fuchs, S., Heiss, K., Huebl, J., 2007. Towards an empirical vulnerability function for use in debris flow risk assessment. Natural Hazards and Earth System Sciences 7, 495–506.

Galli, M., Ardizzone, F., Cardinali, M., Guzzetti, F., Reichenbach, P., 2008. Comparing landslide inventory maps. Geomorphology 94, 268–289.

Ghosh, S., van Westen, C.J., Carranza, E.J.M., Ghoshal, T.B., Sarkar, N.K., Surendranath, M., 2009. A quantitative approach for improving the BIS (Indian) method of medium-scale landslide susceptibility. Journal of the Geological Society of India 74, 625–638.

Ghosh, S., van Westen, C.J., Carranza, E.J.M., Jetten, V.G., 2012a. Integrating spatial, temporal and magnitude probabilities for medium-scale landslide risk analysis in Darjeeling Himalayas, India. Landslides 9, 371–384.

Ghosh, S., van Westen, C.J., Carranza, E.J.M., Jetten, V.G., Cardinali, M., Rossi, M., Guzzetti, F., 2012b. Generating event-based landslide maps in data-scare Himalayan environment for estimating temporal and magnitude probabilities. Engineering Geology 128, 49–62.

Glade, T., 2003. Vulnerability assessment in landslide risk analysis. Beitrag zur Erdsystemforschung 134, 123–146.

GSI, 2006. Landslide Hazard Studies — http://www.gsi.gov.in/lndslde/lhs.htm. Geological Survey of India.

Gumbel, E.J., 1958. Statistics of Extremes. Columbia University Press, New York . (375 pp.).

Guzzetti, F., Cardinali, M., Reichenbach, P., Carrara, A., 2000. Comparing landslide maps: a case study in the upper Tiber River Basin, central Italy. Environmental Management 25, 247–263.

Guzzetti, F., Reichenbach, P., Cardinali, M., Galli, M., Ardizzone, F., 2005. Probabilistic landslide hazard assessment at the basin scale. Geomorphology 72, 272–299.

Jaiswal, P., van Westen, C.J., Jetten, V., 2011. Quantitative assessment of landslide hazard along transportation lines using historical records. Landslides 8, 279–291.

Lu, P., Stumpf, A., Kerle, N., Casagli, N., 2011. Object-oriented change detection for landslide rapid mapping. IEEE Geoscience and Remote Sensing Letters 8, 701–705.

Martha, T.R., Kerle, N., Jetten, V., van Westen, C.J., Vinod Kumar, K., 2010. Characterising spectral, spatial and morphometric properties of landslides for automatic detection using object-oriented methods. Geomorphology 116, 24–36.

Martha, T.R., Kerle, N., van Westen, C.J., Jetten, V., Vinod Kumar, K., 2011. Segment optimisation and data-driven thresholding for knowledge-based landslide detection by object-based image analysis. IEEE Transactions on Geoscience and Remote Sensing 49, 4928–4943.

Martha, T.R., Kerle, N., van Westen, C.J., Jetten, V., Vinod Kumar, K., 2012. Object-oriented analysis of multi-temporal panchromatic images for creation of historical landslide inventories. ISPRS Journal of Photogrammetry and Remote Sensing 67, 105–119.

Mathew, J., Jha, V.K., Rawat, G.S., 2007. Weights of evidence modelling for landslide hazard zonation mapping in part of Bhagirathi Valley, Uttarakhand. Current Science 92, 628–638.

Moine, M., Puissant, A., Malet, J.-P., 2009. Detection of landslides from aerial and satellite images with a semi-automatic method — application to the Barcelonnette basin (Alpes-de-Haute-Provence, France). In: Malet, J.-P., Remaitre, A., Bogaard, T. (Eds.), Landslide Processes: From Geomorphological Mapping to Dynamic Modelling. CERG, Strasbourg, France, pp. 63–68.

Nadim, F., Kjekstad, O., Peduzzi, P., Herold, C., Jaedicke, C., 2006. Global landslide and avalanche hotspots. Landslides 3, 159–173.

Naithani, A.K., 2001. The August, 1998 Okhimath tragedy in Rudraprayag district of Garhwal Himalaya, Uttaranchal, India. Gaia 16, 145–156.

Naithani, A.K., Kumar, D., Prasad, C., 2002. The catastrophic landslide of 16 July 2001 in Phata Byung area, Rudraprayag District, Garhwal Himalaya, India. Current Science 82, 921–923.

Nayak, J., 2010. Landslide risk assessment along a major road corridor based on historical landslide inventory and traffic analysis. MSc Thesis, University of Twente Faculty of Geo-Information and Earth Observation, Enschede, The Netherlands, 104 pp.

Neuhäuser, B., Terhorst, B., 2007. Landslide susceptibility assessment using "weights-of-evidence" applied to a study area at the Jurassic escarpment (SW-Germany). Geomorphology 86, 12–24.

Nichol, J., Wong, M.S., 2005. Satellite remote sensing for detailed landslides inventories using change detection and image fusion. International Journal of Remote Sensing 26, 1913–1926.

Papathoma-Kohle, M., Neuhäuser, B., Ratzinger, K., Wenzel, H., Dominey-Howes, D., 2007. Elements at risk as a framework for assessing the vulnerability of communities to landslides. Natural Hazards and Earth System Sciences 7, 765–779.

Poli, S., Sterlacchini, S., 2007. Landslide representation strategies in susceptibility studies using weights-of-evidence modeling technique. Natural Resources Research 16, 121–134.
Pradhan, B., 2010. Remote sensing and GIS-based landslide hazard analysis and cross-validation using multivariate logistic regression model on three test areas in Malaysia. Advances in Space Research 45, 1244–1256.
Rawat, U.S., Rawat, J.S., 1998. A Report on Geotechnical Reconnaissance of the Excessive Landsliding in August, 1998 near Okhimath, Rudraprayag District, U.P. Technical Report. Geological Survey of India, Northern Region, Lucknow.
Rosin, P.L., Hervas, J., 2005. Remote sensing image thresholding methods for determining landslide activity. International Journal of Remote Sensing 26, 1075–1092.
Sawatzky, D.L., Raines, G.L., Bonham-Carter, G.F., Looney, C.G., 2009. Spatial Data Modeller (SDM): ArcMAP 9.3 geoprocessing tools for spatial data modelling using weights of evidence, logistic regression, fuzzy logic and neural networks. http://arcscripts.esri.com/details.asp?dbid=15341.
Thiery, Y., Malet, J.P., Sterlacchini, S., Puissant, A., Maquaire, O., 2007. Landslide susceptibility assessment by bivariate methods at large scales: application to a complex mountainous environment. Geomorphology 92, 38–59.
van Westen, C.J., Rengers, N., Soeters, R., 2003. Use of geomorphological information in indirect landslide susceptibility assessment. Natural Hazards 30, 399–419.
van Westen, C.J., van Asch, T.W.J., Soeters, R., 2006. Landslide hazard and risk zonation — why is it still so difficult? Bulletin of Engineering Geology and the Environment 65, 167–184.
van Westen, C.J., Castellanos, E., Kuriakose, S.L., 2008. Spatial data for landslide susceptibility, hazard, and vulnerability assessment: an overview. Engineering Geology 102, 112–131.
Varnes, D.J., 1984. Landslide Hazard Zonation: A Review of Principles and Practice. UNESCO, Darantiere, Paris . (61 pp.).
Zêzere, J.L., Garcia, R.A.C., Oliveira, S.C., Reis, E., 2008. Probabilistic landslide risk analysis considering direct costs in the area north of Lisbon (Portugal). Geomorphology 94, 467–495.